Journal of Physics: Conference Series **436** (2013) 012055 doi:10.1088/1742-6596/436/1/012055

Cluster correlations in largely deformed states

Yasutaka Taniguchi
Center for Computational Sciences, University of Tsukuba
1-1-1, Tennodai Tsukuba-city, Ibaraki 305-8577, Japan

E-mail: yasutaka@ccs.tsukuba.ac.jp

Abstract. The coexistence of various deformed states in ^{42}Ca and α–^{38}Ar correlations have been investigated using deformed-basis antisymmetrized molecular dynamics. Wavefunctions of the low-lying states are obtained via parity and angular momentum projections and the generator coordinate method (GCM). Basis wavefunctions of the GCM calculation are obtained via energy variation with constraints on the quadrupole deformation parameter β and the distance between α and ^{38}Ar clusters. The rotational band built on the $J^\pi = 0^+_2$ (1.84 MeV) state as well as the $J^\pi = 0^+_3$ (3.30 MeV) state are both reproduced. The coexistence of two additional $K^\pi = 0^+$ rotational bands is predicted; one band is shown to be built on the $J^\pi = 0^+_3$ state. Members of the ground-state band and the rotational band built on the $J^\pi = 0^+_3$ state contain α–^{38}Ar cluster structure components. The α–^{38}Ar higher-nodal $J^\pi = 0^+$ state is also obtained, and the $J^\pi = 0^+$ state has large E0 transition strength from the ground state.

1. Introduction

Drastic structural changes initiated by low excitation energies are a significant characteristic of nuclear systems, and the coexistence of deformed states and cluster structures is a typical phenomenon. In the mass number region $A \sim 40$, low-lying normal-deformed (ND) and superdeformed (SD) bands with many-particle-many-hole (mp-mh) configurations have been confirmed experimentally. Coupling of the cluster structure components in deformed states such as the α-cluster structure in the ND band of ^{40}Ca [1, 2, 3, 4] and the ground-state band in ^{44}Ti [1, 2, 5] has also be investigated. Recently, enhancement of E0 and IS0 strengths by cluster structure components was discussed [6, 7].

In ^{42}Ca, deformed states with mp-mh configurations and clustering behavior have been observed experimentally, and the rotational band built on the $J^\pi = 0^+_2$ (1.84 MeV) state ($K^\pi = 0^+_2$ band) has been observed [8, 9]. With regard to α-cluster structures, strong population to the $J^\pi = 0^+_1$ and 0^+_3 (3.30 MeV) states has been observed in α-transfer reactions to ^{38}Ar, and the ratios of the cross sections of α and $2n$ transfer reactions suggest that the $J^\pi = 0^+_2$ and 0^+_3 states have configurations of $6p4h$ and $4p2h$, respectively [10]. Theoretically, the α+^{38}Ar orthogonality condition model (OCM) describes $4p2h$ states with α–^{38}Ar cluster structures, but a rotational band with a $6p4h$ configuration is not obtained in low-lying states [11]. To understand the structures in ^{42}Ca, various deformations with mp-mh configurations and clustering should be taken into account, but such a study has never been performed. The structures of low-lying states in ^{42}Ca have not been clarified yet.

This paper aims at clarifying the structures of low-lying positive-parity states in ^{42}Ca by focusing on the coexistence of rotational bands with mp-mh configurations. The α–^{38}Ar cluster correlations in low-lying deformed states are also discussed.

2. Framework

The wavefunctions in low-lying states are obtained using the parity and angular momentum projection (AMP) and the generator coordinate method (GCM) with deformed-basis antisymmetrized molecular dynamics (AMD) wavefunctions. A deformed-basis AMD wavefunction $|\Phi\rangle$ is the Slater determinant of Gaussian wave packets that can deform triaxially such that

$$|\Phi\rangle = \hat{\mathcal{A}}|\varphi_1, \varphi_2, \cdots, \varphi_A\rangle, \quad (1)$$

$$|\varphi_i\rangle = |\phi_i\rangle \otimes |\chi_i\rangle \otimes |\tau_i\rangle, \quad (2)$$

$$\langle \mathbf{r}|\phi_i\rangle = \pi^{-3/4}(\det \mathsf{K})^{1/2} \exp\left[-\frac{1}{2}(\mathsf{K}\mathbf{r} - \mathbf{Z}_i)^2\right], \quad (3)$$

$$|\chi_i\rangle = \chi_i^{\uparrow}|\uparrow\rangle + \chi_i^{\downarrow}|\downarrow\rangle, \ |\tau_i\rangle = |\pi\rangle \text{ or } |\nu\rangle, \quad (4)$$

where $\hat{\mathcal{A}}$ denotes the antisymmetrization operator, and $|\varphi_i\rangle$ denotes a single-particle wavefunction. The $|\phi_i\rangle$, $|\chi_i\rangle$, and $|\tau_i\rangle$ states denote the spatial, spin, and isospin components, respectively, of each single-particle wavefunction $|\varphi_i\rangle$. The real 3×3 matrix K denotes the wave number of the Gaussian single-particle wavefunction that can deform triaxially, which is common to all nucleons. The $\mathbf{Z}_i = (Z_{ix}, Z_{iy}, Z_{iz})$ vectors are complex parameters to denote the centroid of each single-particle wavefunction in phase space. The complex parameters $\chi_i^{\uparrow}$ and $\chi_i^{\downarrow}$ denote the spin directions. Neither time reversal nor axial symmetry are assumed. The basis wavefunctions of the GCM are obtained via the energy variation with two types of constraints: the quadrupole deformation parameter β of the total system and the distance between α and ^{38}Ar clusters, which is defined by the positions of the wave packet centroids [12]. The energy variational calculations are performed after the projection onto positive-parity states. For the energy variation with β, harmonic oscillator (HO) quanta for the protons and neutrons, N_π and N_ν, respectively, relative to the lowest allowed state are also constrained. The variational parameters are K, $\mathbf{Z}_i$, and $\chi_i^{\uparrow,\downarrow}$ $(i = 1, ..., A)$. The isospin component of each single-particle wave function is fixed as a proton (π) or a neutron (ν). The Gogny D1S force is used as the effective interaction. Details of the framework are provided in refs. [13, 14, 12].

3. Results and discussions

Figure 1 shows the energy curves obtained from the energy variation with the constraints on β and the HO quanta N_π and N_ν as functions of β. The HO quanta (N_π, N_ν) are constrained to (0, 0), (2, 0), (2, 2), and (4, 2), which appear on the β–energy curve obtained with the β-constrained energy variation without the HO constraint. The (0, 0), (2, 0), (2, 2), and (4, 2) configurations correspond to the $[(pf)^2]_\nu$, $[(sd)^{-2}(pf)^2]_\pi[(pf)^2]_\nu$, $[(sd)^{-2}(pf)^2]_\pi[(sd)^{-2}(pf)^4]_\nu$, and $[(sd)^{-4}(pf)^4]_\pi[(sd)^{-2}(pf)^4]_\nu$ structures, respectively, which, in total are the $2p$, $4p2h$, $6p4h$, and $8p6h$ configurations. The $4p2h$, $6p4h$, and $8p6h$ states have local minima at $\beta \sim 0.3$, 0.4, and 0.5, respectively. Deformations of the protons and neutrons are similar across the whole β region. The $4p2h$, $6p4h$, and $8p6h$ states form triaxially deformed structures. Through the AMP, largely deformed states gain higher binding energies, and the energy of the local-minimum state for the $6p4h$ configuration projected onto the $J^\pi = 0^+$ state becomes lower than that for $4p2h$ states. The order of the local-minimum energies are the reverse of that before the AMP.

Two kinds of configurations obtained by using energy variation with the intercluster distance constraint are adopted as the GCM basis, and are labeled as A and B. The difference between them is in the orientation of the ^{38}Ar cluster relative to the direction of the α cluster. ^{38}Ar clusters have two proton holes in the *sd*-shell, and the direction of the proton holes is parallel and vertical to the direction of α clusters for configurations A and B, respectively. Superposing those configurations, the rotation of the ^{38}Ar clusters is taken into account partly. Figures 2 and 3

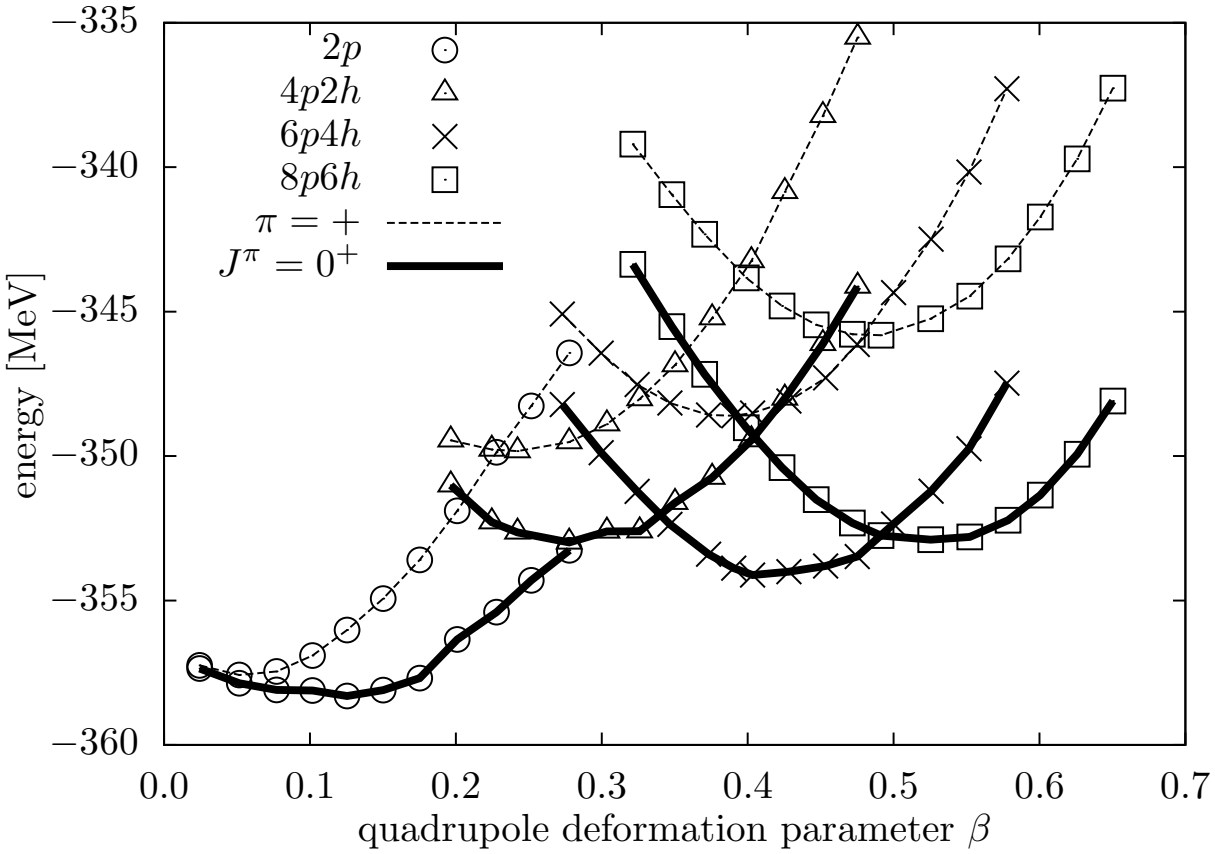

Figure 1. The energy curves as functions of the quadrupole deformation parameter β for positive-parity (solid lines) and $J^\pi = 0^+$ (dashed lines) states. Circles, triangles, crosses, and squares indicate the $2p$, $4p2h$, $6p4h$, and $8p6h$ configurations, respectively (see text).

show the energy and HO quanta, respectively, for the α–^{38}Ar wavefunctions with configuration A and B. In small intercluster distance region the energy of configuration A wave functions go to the ground-state energy, but configuration B is still excited (fig. 2). The excitation of configuration B is caused by $2\hbar\omega$ excitation of the protons. In configuration B the *sd*-shell of protons is fully occupied in the direction of the α cluster, and the protons in the α cluster should be excited to the *pf* shell due to the Pauli blocking effect (fig. 3).

Figure 4 shows the level scheme of the positive-parity states in ^{42}Ca up to the $J^\pi = 8^+$ states obtained via the AMP and the GCM. The GCM bases are deformed-structure wavefunctions with configurations of $2p$, $4p2h$, $6p4h$ and $8p6h$ obtained via energy variation with the β and HO quanta constraints, and α–^{38}Ar cluster structure wavefunctions obtained via energy variation with the α–^{38}Ar intercluster distance constrained to a maximum of 8.5 fm. Convergence of the GCM calculation was confirmed by a comparison with a restricted set of basis wavefunctions (the energies of states listed in fig. 4 change by less than 0.25 MeV when the number of basis wavefunctions is halved). Three $K^\pi = 0^+$ rotational bands coexist in the excited states, labeled as ND1, ND2, and SD. The dominant components of these states have $6p4h$, $4p2h$, and $8p6h$ configurations, respectively, and the quadrupole deformation parameters of their dominant components are $\beta = 0.40$, 0.28 and 0.53, respectively. The ground-state (GS) band has a $2p$ configuration. The theoretical level spacings of the GS band are underestimated, although the GS band is considered to have a simple $[(f_{7/2})^2]_\nu$ structure. The present framework does not

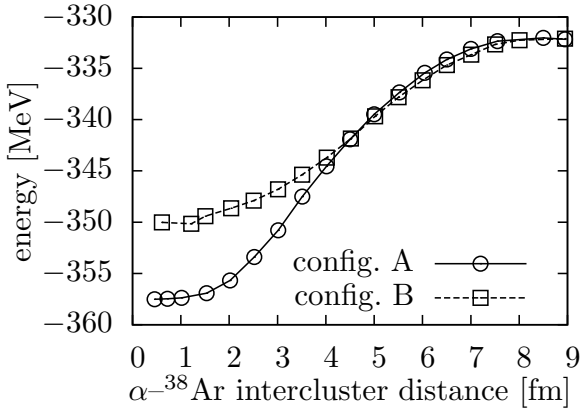

Figure 2. Energy of the α–^{38}Ar wavefunction as the function of the intercluster distance between the α and ^{38}Ar clusters. Solid and dotted lines show configurations A and B, respectively (see text).

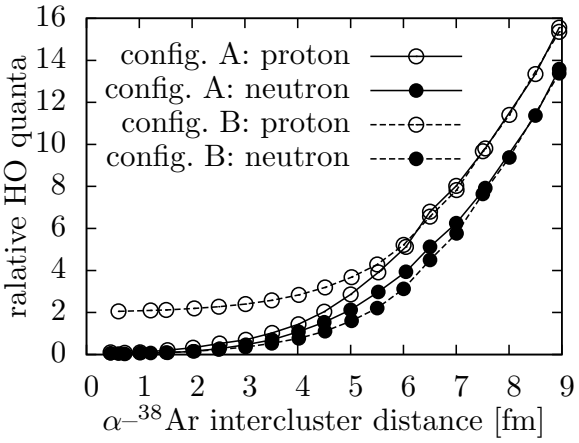

Figure 3. Particle-hole configurations of protons and neutrons relative to the lowest allowed state as the function of the intercluster distance between the α and ^{38}Ar clusters. Solid and dotted lines show configurations A and B, respectively (see text), while open and closed symbols indicate protons and neutrons.

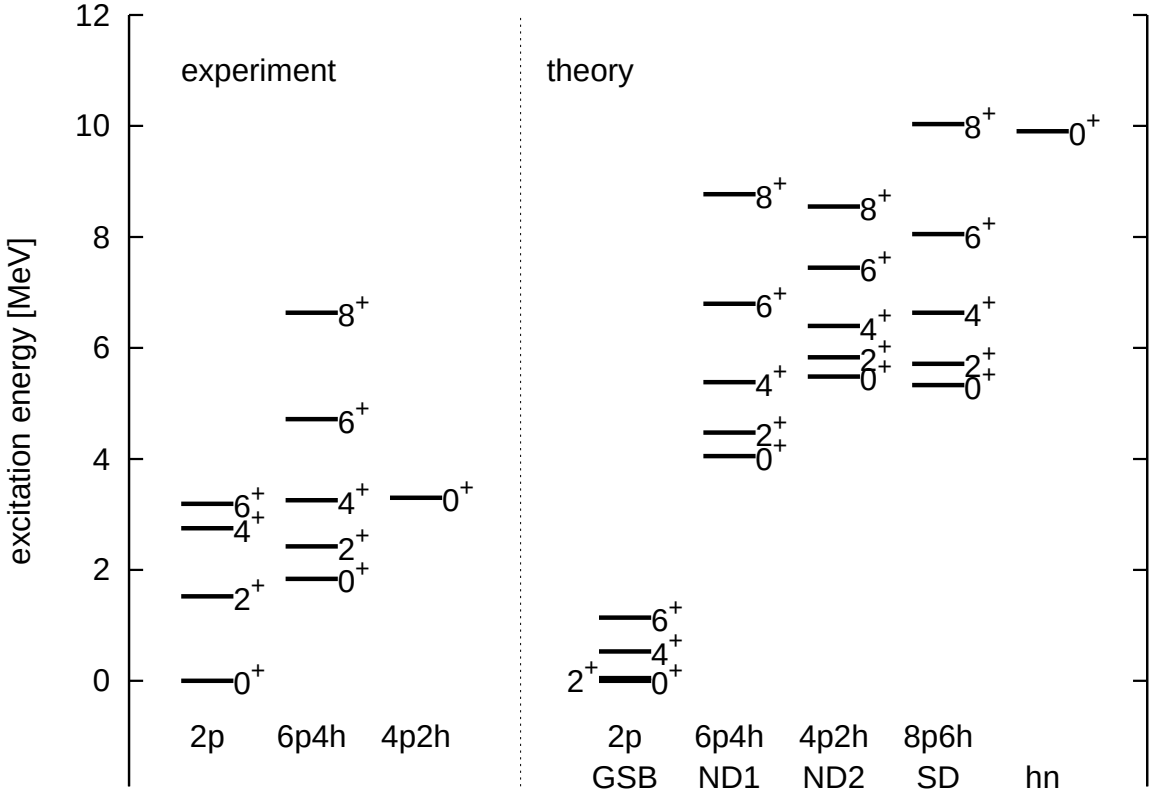

Figure 4. The experimental and theoretical level schemes in ^{42}Ca.

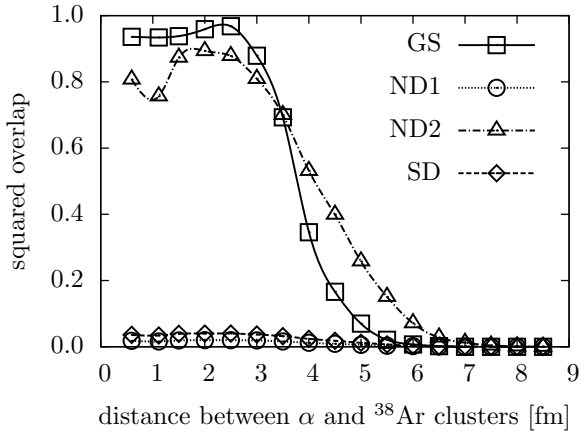

Figure 5. Squared overlaps of the $J^\pi = 0^+_{\rm GS}$ (solid), $0^+_{\rm ND1}$ (dotted), $0^+_{\rm ND2}$ (dot-dashed), and $0^+_{\rm SD}$ (dashed) states as a function of the distance between the α and ^{38}Ar clusters.

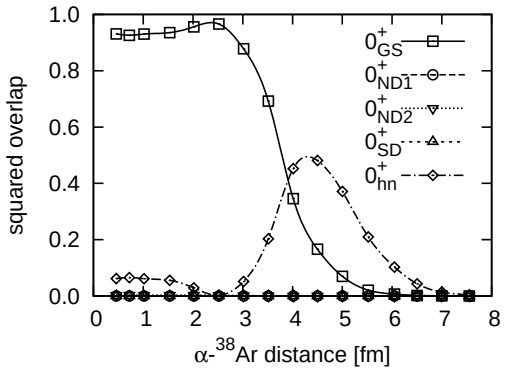

Figure 6. Squared overlaps of the configuration A α–^{38}Ar wavefunctions for the $J^\pi = 0^+_{\rm GS}$ (solid), $0^+_{\rm ND1}$ (dotted), $0^+_{\rm ND2}$ (dot-dashed), and $0^+_{\rm SD}$ (dashed) states as a function of the distance between the α and ^{38}Ar clusters.

include a time-reversal symmetry assumption, and the 2^+ and 4^+ states contain low-energy magnetized components, which leads to the underestimation. In the highly excited region a 0^+ state that contains large amount of α–^{38}Ar cluster structure components is obtained, which has α–^{38}Ar higher-nodal (hn) structure as discussed below.

To analyze the α–^{38}Ar cluster structure correlations in the low-lying rotational bands, squared overlaps of the band-head states and α–^{38}Ar cluster structure components were calculated, as shown in fig. 5. The squared overlaps of the $J^\pi = 0^+_{\rm GS}$, $0^+_{\rm ND1}$, $0^+_{\rm ND2}$, and $0^+_{\rm SD}$ states, which are band heads of the GS, ND1, ND2, and SD bands, respectively, are shown with the space spanned by α–^{38}Ar cluster structure wave functions obtained via energy variation with the α–^{38}Ar cluster distance constraint. In the calculations, two types of α–^{38}Ar cluster structure wavefunctions are obtained that differ in the orientation of the ^{38}Ar clusters. The $J^\pi = 0^+_{\rm GS}$ and $0^+_{\rm ND2}$ states have large amount of α–^{38}Ar cluster structure components at large intercluster distances as well as at small distances. The $J^\pi = 0^+_{\rm ND1}$ and $0^+_{\rm SD}$ states have small amount of α–^{38}Ar cluster structure components for any intercluster distance.

B(E2) values of transitions within the theoretical ND1, ND2 and SD bands, as well as within the experimental $K^\pi = 0^+_2$ band are listed in table 1 in Weisskopf units. The B(E2) values of ND1 and ND2 are similar, while those of the SD band are much larger. The theoretical values for the ND1 and ND2 bands are also similar to the experimental values for the $K^\pi = 0^+_2$ band.

The amount of α–^{38}Ar cluster components (fig. 5) and the in-band transition B(E2) values (table 1) indicate that the ND1 band and the band head of the ND2 band correspond to the experimental $K^\pi = 0^+_2$ band and $J^\pi = 0^+_3$ state, respectively. The large amount of α–^{38}Ar cluster components in the $J^\pi = 0^+_{\rm ND2}$ state reveals that this state corresponds to the experimental $J^\pi = 0^+_3$ state because of strong population to the $J^\pi = 0^+_3$ state by α-transfer reactions to ^{38}Ar [10], which is sensitive to the α–^{38}Ar cluster structure components. The ND1 states have small amount of α–^{38}Ar cluster structure components and similar in-band B(E2) values to those of the experimental $K^\pi = 0^+_2$ band, which indicates that the ND1 band corresponds to the experimental $K^\pi = 0^+_2$ band. The particle-hole configurations of the ND1 ($6p4h$) and ND2 ($4p2h$) bands are consistent with those of the $J^\pi = 0^+_2$ and 0^+_3 states, respectively, as suggested by the results of an α-transfer experiment [10]. The members of the ND2 band apart from the band head and

Table 1. Theoretical and experimental B(E2) values in Weisskopf units (I_i and I_f indicate initial and final states, respectively). Experimental values are taken from refs. [8] and [15].

	I_i	I_f	B(E2)
theory	$2^+_{\rm ND1}$	$0^+_{\rm ND1}$	28.55
	$4^+_{\rm ND1}$	$2^+_{\rm ND1}$	33.12
	$6^+_{\rm ND1}$	$4^+_{\rm ND1}$	38.45
	$2^+_{\rm ND2}$	$0^+_{\rm ND2}$	29.02
	$4^+_{\rm ND2}$	$2^+_{\rm ND2}$	24.70
	$6^+_{\rm ND2}$	$4^+_{\rm ND2}$	24.61
	$2^+_{\rm SD}$	$0^+_{\rm SD}$	82.12
	$4^+_{\rm SD}$	$2^+_{\rm SD}$	107.99
	$6^+_{\rm SD}$	$4^+_{\rm SD}$	130.18
experiment	4^+_2	2^+_2	57 ± 42
($K^\pi = 0^+_2$ band)	6^+_2	4^+_2	50^{+35}_{-16}

Table 2. Theoretical and experimental values of electric monopole strengths $M(\mathrm{E0})_{\rm th}$ and $M(\mathrm{E0})_{\rm exp}$, respectively, from the ground state. The unit is in e fm^2. Theoretical values are taken from Ref. [15].

		in e fm^2
transition	$M(E0)_{\rm th}$	$M(E0)_{\rm exp}$
$0^+_{\rm ND1}$	0.09	5.24 ± 0.39
$0^+_{\rm ND2}$	0.52	
$0^+_{\rm SD}$	0.11	
$0^+_{\rm hn}$	4.48	

those of the SD band have not been observed. The members of the ND2 band could possibly be observed by a combination of α-transfer reactions and γ-spectroscopy experiments because the ND2 band contains large amount of α–^{38}Ar cluster structure components and has large in-band B(E2) values.

Table 2 shows E0 transition strengths [M(E0)] from the ground state. The $0^+_{\rm hn}$ has large E0 value compared with other states. It is because the $0^+_{\rm hn}$ state and the ground state contain large amount of the configuration A α–^{38}Ar cluster structure components. Figure 6 shows squared overlaps of the configuration A α–^{38}Ar cluster wavefunctions as a function of the intercluster distance. The ground state and the $0^+_{\rm hn}$ state contains large amount of the configuration A α–^{38}Ar cluster structure components with small and large intercluster distance, respectively. It shows that the $0^+_{\rm hn}$ state has a α–^{38}Ar higher-nodal structure. The α–^{38}Ar cluster structures in the ground state and the $0^+_{\rm hn}$ state enhance E0 transition strengths because E0 transitions excite intercluster motion [6, 7].

The M(E0) of the $0^+_{\rm ND1}$ state underestimates the experimental data. A possible reason is that cluster structure components other than the α–^{38}Ar cluster structure are insufficient in the present calculation. The structure of α + ^{36}Ar with two neutrons in molecular orbitals is a candidate cluster structure coupled in the $0^+_{\rm ND1}$ state. The structure of α + ^{36}Ar with two neutrons in molecular orbitals probably contains α–^{38}Ar cluster structure components, and the

$0^+_{\rm ND1}$ state is also populated by the α-transfer reactions to ^{38}Ar, although the population is weaker than that of the ND2 states.

4. Conclusions

The structures of the deformed states in ^{42}Ca have been investigated using deformed-basis AMD and the GCM by focusing on the coexistence of various rotational bands with mp-mh configurations and α–^{38}Ar clustering. In the excited states, three $K^\pi = 0^+$ bands, ND1, ND2 and SD were obtained, which have dominant $6p4h$, $4p2h$, and $8p6h$ configurations, respectively. The ND1 band corresponds to the experimental $K^\pi = 0^+_2$ band, while the ND2 and SD bands have not yet been observed. The band head of the ND2 band corresponds to the experimental $J^\pi = 0^+_3$ state. The B(E2) values of the in-band transitions of the ND1 band are consistent with experimental data. The members of the GS and ND2 bands contain α–^{38}Ar cluster structure components, which is consistent with results that show the $J^\pi = 0^+_1$ and 0^+_3 states are strongly populated by ^{38}Ar(^{6}Li, d) reactions. Particle-hole configurations of the dominant components of the GS and ND2 bands are consistent with the suggestions of the α-transfer to ^{38}Ar experiment. The α–^{38}Ar higher-nodal state is also obtained, which has large E0 strength from the ground state. It is necessary to consider both clustering and various deformations with mp-mh configurations for understanding the structures in ^{42}Ca.

Acknowledgments

This work was supported by the University of Tsukuba Research Infrastructure Support Program. Numerical calculations were conducted on the RIKEN Integrated Cluster of Clusters (RICC) and the "Interdisciplinary Computational Science Program" in Center for Computational Sciences, University of Tsukuba.

References

[1] Michel F, Ohkubo S and Reidemeister G 1998 *Prog. Theor. Phys. Suppl.* **132** 7 and references therein
[2] Yamaya T, Katori K, Fujiwara M, Kato S and Ohkubo S 1998 *Prog. Theor. Phys. Suppl.* **132** 73 and references therein
[3] Sakuda T and Ohkubo S 1998 *Prog. Theor. Phys. Suppl.* **132** 103 and references therein
[4] Taniguchi Y, Kimura M, Kanada-En'yo Y and Horiuchi H 2007 *Phys. Rev.* C **76** 044317
[5] Kimura M and Horiuchi H 2006 *Nucl. Phys.* A **767** 58
[6] Kawabata T *et al* 2007 *Phys. Lett.* B **646** 6
[7] Yamada T, Funaki Y, Horiuchi H, Ikeda K and Tohsaki A 2008 *Prog. Theor. Phys.* **120** 1139
[8] Betz P, Bitterwolf E, Busshardt B and Röpke H 1976 *Z. Phys.* A **276** 295
[9] Lach M *et al* 2003 *Eur. Phys. J.* A **16** 309
[10] Fortune H, Betts R, Bishop J, AL-Jadir M and Middleton R 1978 *Nucl. Phys.* A **294** 208
[11] Sakuda T and Ohkubo S 1995 *Phys. Rev.* C **51** 586
[12] Taniguchi Y, Kimura M and Horiuchi H 2004 *Prog. Theor. Phys.* **112** 475
[13] Kanada-En'yo Y and Horiuchi H 1995 *Prog. Theor. Phys.* **93** 115
[14] Kimura M 2004 *Phys. Rev.* C **69** 044319
[15] Cameron J A and Singh B 2004 *Nuclear Data Sheets* **102** 293